PERGAMON

International Journal of Heat and Mass Transfer 42 (1999) 2313–2325

International Journal of HEAT and MASS TRANSFER

Double-diffusive convection in an annular vertical porous layer

M. Marcoux*, M.-C. Charrier-Mojtabi, M. Azaiez

Institut de Mécanique des Fluides de Toulouse, UMR no. 5502 CNRS/INP/UPS, Université Paul Sabatier, 118 route de Narbonne, 31062 Toulouse, France

Received 31 October 1996; in final form 30 September 1998

Abstract

This paper reports an analytical and numerical study of double-diffusive natural convection through a fluid-saturated, vertical and homogeneous porous annulus subjected to uniform fluxes of heat and mass from the side. The influence of each leading parameter and especially curvature, a major parameter of this geometry, has been numerically investigated. Solutions are presented for $1 \leqslant A \leqslant 10$, $1 \leqslant Ra_T \leqslant 200$, $1 \leqslant Le \leqslant 20$, $0.1 \leqslant N \leqslant 10$ and $0 \leqslant \gamma \leqslant 10$ where A, Ra_T, Le, N and γ denote the aspect ratio, thermal Rayleigh number, Lewis number, buoyancy ratio and curvature parameter, respectively. For the steady state, an analytical solution valid for stratified flow in slender enclosures is presented. A good agreement is observed between the analytical predictions and the numerical simulation for sufficiently high aspect ratios.

Nomenclature

A aspect ratio $= H/e$
C concentration
c_p specific heat at constant pressure
D mass diffusivity
$2e$ enclosure width $= r_o - r_i$
$2H$ enclosure height
j' lateral mass fluxes
Le Lewis number
N buoyancy ratio
Nu average Nusselt number
P pressure
q' lateral heat fluxes
r, z cylindrical polar coordinates
Ra_T thermal Rayleigh number
Sh average Sherwood number
T temperature
U, W filtration velocity components.

Greek symbols
α thermal diffusivity
β_T thermal expansion coefficient
β_C concentration expansion coefficient
γ curvature parameter $= e/r_i$
ε porosity of the porous medium
κ characteristical permeability
λ thermal conductivity
μ dynamic viscosity
ν kinematic viscosity $= \mu/\rho_0$
ρ density
σ heat capacity ratio.

Subscripts
i inner cylinder
o outer cylinder.

1. Introduction

The phenomenon of natural convection through porous media has been studied extensively in the past (Combarnous and Bories [1]) and the recent book of Nield and Bejan [2] summarizes the state of the art. However, in fluid mixtures saturating the porous media, where the variation of fluid density is induced by both temperature and solute (the so-called double-diffusive flow), the dynamics of heat and mass transfer can be very different from those driven by the temperature field alone.

* Corresponding author. E-mail: marcoux@lm2f.ups-tlse.fr

0017–9310/99/$ - see front matter
PII: S0017–9310(98)00332–9

A major part of the fundamental research on double diffusive convection has been reviewed by Trevisan and Bejan [3].

Interest in this phenomenon, driven by the combined buoyancy effect due to temperature and concentration variations through the porous medium, has lately been motivated by the involvement of the process in such diverse problems as contaminant transport in saturated soils, the underground disposal of nuclear waste and the migration of moisture in fibrous insulation.

Studies in double-diffusion in porous media primarily focus on the problem of convective instability in a horizontal layer. Many authors have investigated this problem theoretically, experimentally and numerically; an overview of these earlier works is also in [2] and [3]. However, because the most basic geometry for the study of simultaneous heat and mass transfer from the side is the vertical wall, most of the available studies dealing with double-diffusive natural convection in confined porous media concern rectangular cavities subjected to constant gradients of temperature and solute concentration at their vertical walls. For this vertical configuration, the first investigations concerned the stability of compositional and thermally stratified layers (Gershuni et al. [4], Khan and Zebib [5]) and boundary layer flow (Bejan and Khair [6]). This case allows the development of closed-form analytical solutions for engineering heat and mass transfer calculations and the improvement of the order-of-magnitude estimates produced by scale analysis. References [7–15] concern the theoretical and numerical papers published during the past decade on this subject. Trevisan and Bejan [7] developed, in 1986, an analytical Oseen-linearized solution for the boundary layer regime, valid for the case $Le = 1$, and a similarity solution for the heat-driven flow limit and $Le > 1$. They also performed an extensive series of numerical experiments that validate the analytical results and provide heat and mass transfer data in the domain not covered by analysis. Zhang and Bejan [8] carried out, in 1987, a two-dimensional study of the spreading rate of an isolated porous medium contaminated by the deposition of both thermal and chemical wastes. Scale analysis and numerical methods were used to predict the distinct regimes and respective heat and mass transfer scales for the two extreme cases of heat-driven and solute-driven natural convection. A closed-form analytical solution was also developed for the limit of infinitely shallow layers. Alavyoon and co-workers re-examined in 1993 [9] and 1994 [10] the case considered by Trevisan and Bejan [7] for co-operative ($N > 0$) [9] and opposing ($N < 0$) buoyancy forces [10]. They presented an analytical solution valid for stratified flow in slender enclosures ($A \gg 1$) and a scale analysis that agrees with approximations of the analytical solution within the heat-driven and solute-driven limits. Comparisons between fully numerical and analytical solutions are presented for a wide range of parameters, as well as a domain in which oscillating convection is obtained [10]. A numerical study by Lin in 1993 [11] analysed transient natural convection heat and mass transfer in a square porous enclosure. He shows that an increase of the buoyancy ratio N improves heat and mass transfer and causes the flow to approach steady-state condition in a short time. In 1995, Mamou et al. [12] numerically studied the case of an inclined slot and developed an analytical solution for parallel flows in the core of the cavity. They also showed numerically [13] that in a square enclosure ($A = 1$) where the two buoyancy forces counteract each other ($N = -1$), the problem should have multiple steady state solutions. Very recently, Mamou et al. [14] and Marcoux et al. [15] studied the stability of this particular configuration of double-diffusion in a porous vertical cavity with opposing thermal and solutal buoyant forces. They investigated, numerically and analytically, the onset of convection and the existence of a critical Rayleigh value above which convection occurs.

All these studies mainly focused on two-dimensional rectangular cavities. Such models do not always adequately represent the more practical situations in which the cavity is a porous layer bounded by two vertical concentric cylinders exposed to uniform fluxes of heat and mass. Flow structure and convective heat transfer, in a vertical annular porous layer under the condition of constant heat flux or isothermal heating and cooling along the vertical side walls, have been analysed earlier both numerically and experimentally, but only for natural convection with a single component. The works by Havstad and Burns in 1982 [16] and Hickox and Gartling in 1984 [17] are both theoretical and consider an isothermally heated annulus whose outer wall is cooled to a constant temperature, the top and the bottom walls being insulated. By numerical, perturbation and asymptotic methods, they obtained results for a wide range of parameters. Reda, in 1985 [18], conducted experiments for a water-glass filled vertical annulus with the inner wall heated by applying a constant heat flux and reported the temperature distributions and heat transfer results for Rayleigh numbers up to 80. Prasad and co-workers, during the years 1984–86, conducted a series of numerical [19, 20] and experimental [21, 22] studies. Their numerical studies indicate effects of curvature and Prandtl number on temperature profiles and Nusselt numbers, and experimental data support most of the conclusions derived from the theoretical studies. On the basis of a parallel flow model, Nguyen et al. [23] obtained, in 1986, a closed-form solution for the temperature and the velocity distributions in the pseudo-conduction as well as boundary layer flow regime. It has been validated with numerical solutions.

The purpose of the present report is to make up for this lack of studies concerning this geometry by analysing double-diffusive convection in a vertical annular porous

layer filled with a two-component mixture and subjected to heat and mass fluxes at the vertical boundaries. In the first part, the system of equations leading this problem was solved numerically to obtain a detailed description of the velocity, temperature and concentration within the cavity in order to emphasise the influence of the dimensionless parameters Ra_T, Le, N and curvature on steady and unsteady convective flows. For the case of high aspect ratios ($A \geqslant 5$), an analytical solution is proposed on the basis of a parallel flow model. The good agreement of this solution with the numerical results shows that the analytical model can be faithfully used to obtain a concise description of the problem for these cases.

2. Problem statement

Consider a layer of thickness $2e$ and height $2H$ under normal gravity bounded by two vertical concentric cylinders filled with a homogeneous isotropic porous medium saturated by a two-component incompressible fluid, as shown in Fig. 1.

Both cylinders are exposed to uniform fluxes of heat (q_i', q_o') and mass (j_i', j_o'), while the horizontal walls are regarded as being insulated and impermeable.

It should be noticed that in this kind of configuration, there is another parameter in addition to the aspect ratio $A = H/e$ characterizing the geometry that is $\gamma = e/r_i$, where $0 < \gamma < \infty$. This parameter allows quantification of the curvature effects. So, a value of zero of γ (infinitely wide curvature) implies that the behaviour of the mixture matches that of a rectangular geometry, and, similarly, the effect of curvature increases with increasing γ.

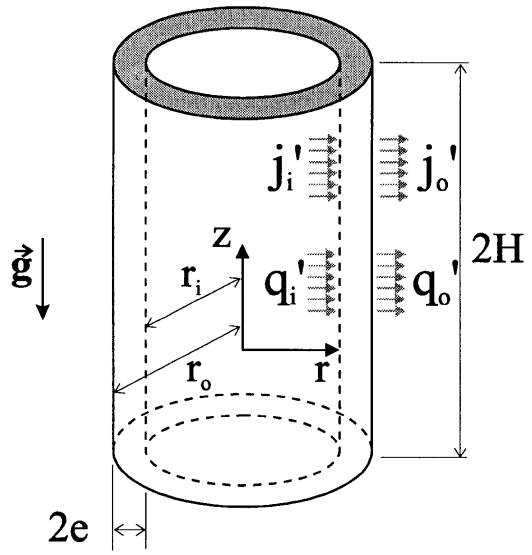

Fig. 1. Geometry of the porous enclosure subjected to uniform heat and mass fluxes in the horizontal direction.

By a porous medium we mean a material consisting of a solid matrix of physical–chemical characteristics ($\varepsilon, \kappa, (\rho c)_s, \lambda_s$) saturated by a fluid, a two-component mixture in our case, represented by the parameters ($\nu, (\rho c_p)_f, \lambda_f, D$). The whole porous medium can be treated as a continuum with the solid and fluid phases and can be modelled as a fictitious isotropic and homogeneous medium with properties ($\lambda^*, (\rho c)^*, D^*$) which can be obtained by composition laws or taking the tortuosity τ of the pore structure into account.

The classical hypotheses used in this study are:

—the Dufour effect (heat flux produced by concentration gradient) is ignored.

—the Soret effect (mass flux produced by temperature gradient) is ignored. This assumption is not always valid for mixture (Marcoux et al. [24]).

—the fluid is assumed to be a Boussinesq fluid: i.e. both the porous matrix and the saturating fluid are incompressible, and all thermo-physical properties of the medium are constant, except the density of the mixture which depends linearly on the temperature and the concentration, and is given by

$$\rho(T, C) = \rho_o[\mathbf{1} - \beta_T(T - T_o) - \beta_C(C - C_o)]. \quad (1)$$

The equations governing the conservation of mass, momentum in the Darcy regime, energy and solute concentration in the porous medium have been reduced to dimensionless forms by using the following scales: L for length, $V_o = \alpha/L$ for velocity, $t_o = \sigma L^2/\alpha$ for time, $P_o = \alpha\nu\rho_0/\kappa$ for pressure, $\delta T = (q_i')L/\lambda^*$ for temperature and $\delta C = j_i' L/D^*$ for concentration, with $\sigma = (\rho c)^*/(\rho c_p)_f$ and $\alpha = \lambda^*/(\rho c_p)_f$.

The non-dimensional version of the problem to be considered reads, using vectorial notations:

$$\nabla \cdot \mathbf{V} = 0 \quad (2)$$

$$\mathbf{V} = -\nabla P + Ra_T(T + NC)\mathbf{e}_z \quad (3)$$

$$\frac{\partial T}{\partial t} + (\mathbf{V} \cdot \nabla)T = \nabla^2 T \quad (4)$$

$$\varepsilon^* \frac{\partial C}{\partial t} + (\mathbf{V} \cdot \nabla)C = \frac{1}{Le}\nabla^2 C. \quad (5)$$

Then, the dimensionless parameters governing double-diffusive natural convection are the Rayleigh number, Ra_T, the normalized porosity, ε^*, the Lewis number, Le, and the buoyancy ratio, N, defined by:

$$Ra_T = \frac{\beta_T g \kappa}{\nu\alpha} L\delta T \quad (6)$$

$$\varepsilon^* = \frac{\varepsilon}{\sigma} \quad (7)$$

$$Le = \frac{\alpha}{D^*} \quad (8)$$

$$N = \frac{Ra_c}{Ra_T} = \frac{\beta_c \delta C}{\beta_T \delta T}. \quad (9)$$

They are completed with the aspect ratio A and the curvature parameter γ described previously.

For this case of cylindrical geometry, we are mainly concerned with two-dimensional flows, and the problem can be reduced to axisymmetrical coordinates (r, z) (Fig. 2).

The length scale L is the half thickness e of the vertical layer between the two cylinders. The dimensionless slot is then defined by the aspect ratio and the inner and outer radii, the latter depending on the curvature parameter: $r_i = 1/\gamma$ and $r_o = 2 + 1/\gamma$. With the following decomposition for the velocity: $\mathbf{V}(r, z) = U(r, z)\mathbf{e}_r + W(r, z)\mathbf{e}_z$, the governing equations (6)–(9) can be reduced to the set of equations below:

$$\frac{1}{r}\frac{\partial}{\partial r}(rU) + \frac{\partial}{\partial z}W = 0 \quad (10)$$

$$U = -\frac{\partial P}{\partial r} \quad W = -\frac{\partial P}{\partial z} + Ra_T(T + NC) \quad (11)$$

$$\frac{\partial T}{\partial t} + U\frac{\partial T}{\partial r} + W\frac{\partial T}{\partial z} = \frac{1}{r}\frac{\partial}{\partial r}\left(r\frac{\partial T}{\partial r}\right) + \frac{\partial^2 T}{\partial z^2} \quad (12)$$

$$\varepsilon^* \frac{\partial C}{\partial t} + U\frac{\partial C}{\partial r} + W\frac{\partial C}{\partial z} = \frac{1}{Le}\left[\frac{1}{r}\frac{\partial}{\partial r}\left(r\frac{\partial C}{\partial r}\right) + \frac{\partial^2 C}{\partial z^2}\right]. \quad (13)$$

The appropriate boundary conditions are: $U(r = r_i, z) = U(r = r_o, z) = 0$, $W(r, z = \pm A) = 0$,

$$\left.\frac{\partial T}{\partial r}\right|_{r=r_i} = \left.\frac{\partial C}{\partial r}\right|_{r=r_i} = 1, \quad \left.\frac{\partial T}{\partial r}\right|_{r=r_o} = \left.\frac{\partial C}{\partial r}\right|_{r=r_o} = \frac{1}{2\gamma + 1}$$

$$\text{and} \quad \left.\frac{\partial T}{\partial z}\right|_{z=\pm A} = 0 \quad \left.\frac{\partial C}{\partial z}\right|_{z=\pm A} = 0. \quad (14)$$

Actually, in order to satisfy heat and mass conservation, the inner and outer heat and mass fluxes are related by $q_i' r_i = q_o' r_o$ and $j_i' r_i = j_o' r_o$.

Equations (10)–(13), together with the boundary conditions (14), then completely determine the problem in terms of the dimensionless parameters $(A, \gamma, Ra_T, Le, N, \varepsilon^*)$.

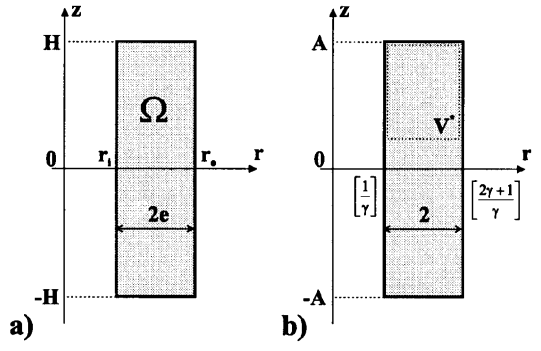

Fig. 2. Schema of a two-dimensional porous layer in the axisymmetrical (a) and non-dimensional form (b).

As the problem is two-dimensional and incompressible, one can introduce the stream function Ψ, defined by:

$$U = \frac{-1}{r}\frac{\partial \Psi}{\partial z} \quad \text{and} \quad W = \frac{1}{r}\frac{\partial \Psi}{\partial r}.$$

Thus, upon the introduction of the stream function, equations (10) and (11) get replaced by:

$$\frac{\partial^2 \Psi}{\partial r^2} - \frac{1}{r}\frac{\partial \Psi}{\partial r} + \frac{\partial^2 \Psi}{\partial z^2} = r\,Ra_T\left(\frac{\partial T}{\partial r} + N\frac{\partial C}{\partial r}\right)$$

$$\text{with} \quad \Psi = 0 \quad \text{on } \partial\Omega. \quad (15)$$

3. Numerical solution

The complete governing equations (10)–(14) were solved via spectral collocation methods, especially efficient for partial derivative problems in simple geometries (Azaiez et al. [25]). Unlike classical methods like finite differences or finite volume methods, spectral methods are global; in particular, the spatial derivative value of a function at one point depends on the values of the function at all the nodes of the grid. This particularity allows the use of a relatively small mesh size. Another advantage of these methods concerns their great precision; actually, the approximation error size is only limited by the regularity of the exact solution. The accuracy of spectral approximations comes from the rapid (exponential) decay of approximation errors as the spectral resolution is increased. Compared to the relatively slow (algebraic) convergence typical of finite difference or finite element methods, far more efficient numerical simulations can be achieved (Canuto et al. [26]).

The spatial discretization of the problem by spectral methods is a technique involving the resolution of partial derivative equations based on the approximations of the solution by high-degree polynomials and the use of a polynomial tensorial basis. These methods consist of numerical integration by quadratic formulae:

$$\forall \Phi \in P_{2N-1}, \quad \exists ! \{\xi_i, \rho_i\}_N: \quad \int_{-1}^{1} \Phi(x)\,dx = \sum_{i=0}^{N} \Phi(\xi_i)\rho_i. \quad (16)$$

The collocation points (ξ_i) chosen for spatial discretization are the Gauss–Lobatto–Legendre points, defined as solutions of the equation: $(1 - x^2)L_n'(x) = 0$ where, $L_n(x)$ are the Legendre polynomials, orthogonal on $L^2[-1, 1]$. These points have the property that the solution is exact for any polynomial function of degree $\leqslant 2N - 1$, and the node distribution becomes squeezed near the edges, so this mesh pattern is specially indicated in such problems where boundary layers occur.

Temporal integration is made by a backward Adams–Bashforth/Euler scheme, a second-order discretization, that implicitly solves the diffusion term and explicitly the convection terms:

$$\left(\frac{\partial T}{\partial t}-\nabla^2 T\right)^{n+1}=\frac{3T^{n+1}/2-2T^n+T^{n-1}/2}{\Delta t}-\nabla^2 T^{n+1} \tag{17}$$

$$(\mathbf{V}\cdot\nabla T)^{n+1}=2\mathbf{V}^n\cdot\nabla T^n-\mathbf{V}^{n-1}\cdot\nabla T^{n-1}. \tag{18}$$

The complete discretization of our problem leads to the resolution of two-classical differential problems. The first is the Helmholtz problem that concerns the unsteady conservation equations (12) and (13), in which the unknown variables are T and C and where the association to Neuman's boundary conditions (14) implies the use of a variational formulation called weak. The other is the Darcy problem constituted by equations (10) and (11), whose unknowns are U, W and P and which is solved by the Uzawa algorithm (Arrow et al. [27]). This set of equations reduces, in the spectral space, to a Poisson's tensional linear system that can be easily solved by the direct method of successive diagonalization (Zang et al. [28]).

From a set of $(A, \gamma, Ra_T, Le, N, \varepsilon^*)$ parameters and an initial field of values, we can thus obtain the temporal variation of the variables (T, C, U, W, P). The solution is assumed to have reached the steady state as soon as the residue (difference between two successive estimates of any variable) satisfies the following criterion:

$$\mathrm{Res}(\varphi)=\max_{\Omega}|\varphi^{k+1}-\varphi^k|<10^{-6},$$

where φ denotes any of the five quantities (T, C, U, W, P), and the subscript k indicates the time-step order.

In most engineering applications, where the details of the solution are of less significance, the overall solute and heat transfer rate of the system under consideration is summarized by resorting to the Nusselt and Sherwood numbers. The average Nusselt and Sherwood numbers at the inner and outer cylinders are defined respectively by:

$$Nu_i=\left(\frac{q'_{\mathrm{convect}}}{q'_{\mathrm{conduct}}}\right)_{r_i}=2A\frac{\ln(2\gamma+1)}{\gamma}\left(\int_{-A}^{+A}\Delta T\,\mathrm{d}z\right)^{-1}$$
$$\text{and}\quad Nu_o=(2\gamma+1)Nu_i \tag{19}$$

$$Sh_i=\left(\frac{j'_{\mathrm{convect}}}{j'_{\mathrm{conduct}}}\right)_{r_i}=2A\frac{\ln(2\gamma+1)}{\gamma}\left(\int_{-A}^{+A}\Delta C\,\mathrm{d}z\right)^{-1}$$
$$\text{and}\quad Sh_o=(2\gamma+1)Sh_i \tag{20}$$

where ΔT and ΔC are the side-to-side temperature and concentration differences.

This program, dealing with the problem of double-diffusive convection in a cylindrical geometry, has been successfully tested with results from other authors either in natural convection ($N=0$) for the same geometry [4, 5] or in double-diffusive convection for a rectangular geometry (γ small enough) [6–9].

Examinations of the numerical results led to some assumptions about flow behaviour for high aspect ratios that will afterwards allow us to solve the problem analytically.

4. Analytical solution for the steady-state

4.1. Formulation

The numerical solution to the full problem indicates that when the momentum, heat and mass balance in the enclosure can be represented by a slow progression towards a steady state, the temperature and concentration fields become linearly and stably stratified in the vertical direction, for sufficiently high aspect ratios (see Section 5).

In these cases, outside the end regions, the velocity vector proves to be predominantly vertical. Guided by these observations, the proposed form of the steady-state analytical solution reads:

$$\mathbf{V}(r,z)=W(r,z)\mathbf{e}_z\quad T(r,z)=\theta(r)+\alpha(z)$$
$$C(r,z)=\phi(r)+\beta(z)$$

where W, θ, ϕ, α, β are unknown functions to be determined.

According to these assumptions, equations (10) and (11) imply that W is independent of the vertical coordinate z and P is independent of the radial coordinate r: $W\equiv W(r)$, $P\equiv P(z)$. Introducing these relationships into equations (10)–(14) and rearranging the terms, a system of second-order ordinary differential equations is obtained:

$$W-Ra_T(\theta+N\phi)=-P'+Ra_T(\alpha+N\beta) \tag{21}$$

$$W\alpha'=\Delta_r\theta+\alpha'' \tag{22}$$

$$W\beta'=\frac{1}{Le}(\Delta_r\phi+\beta'') \tag{23}$$

where Δ_r is the radial component of the Laplacian:

$$\Delta_r=\frac{1}{r}\frac{\partial}{\partial r}\left(r\frac{\partial}{\partial r}\right)\quad\text{and}\quad f'(r)=\frac{\mathrm{d}f}{\mathrm{d}r}.$$

It can be already noticed that the left hand of equation (21) is only dependent on r and the right hand on z, so the variables can be separated, which implies:

$$W-Ra_T(\theta+N\phi)=Cste=k$$
$$\text{and}\quad P'-Ra_T(\alpha+N\beta)=-k.$$

The associated boundary conditions are:

$$\theta'(r_i)=\phi'(r_i)=1\quad\text{and}\quad\theta'(r_o)=\phi'(r_0)=\frac{1}{2\gamma+1}. \tag{24}$$

By solving equations (21)–(23), which are subjected to

boundary conditions (24), the unknown functions can be determined in terms of five integration constants (k, C_1, C_2, D_1, D_2). To do so, five other conditions have to be imposed on the solution.

4.2. Additional conditions

4.2.1. Conservation of mass

Mass is conserved across any transversal section:

$$\int_{r_i}^{r_o} W(r) r \, dr = 0. \tag{25}$$

4.2.2. Conservation of total amount of solute

As the problem studied here includes neither chemical reactions nor mass and thermal sources, there is no production or waste of any of the components. The total amount of solute has, therefore, to be conserved:

$$2A \int_{r_i}^{r_o} \phi(r) r \, dr + 2(1+1/\gamma) \int_{-A}^{A} \beta(z) \, dz = 0. \tag{26}$$

4.2.3. Conservation of total enthalpy

With a similar reasoning, the conservation of total enthalpy leads to:

$$2A \int_{r_i}^{r_o} \theta(r) r \, dr + 2(1+1/\gamma) \int_{-A}^{A} \alpha(z) \, dz = 0. \tag{27}$$

4.2.4. Balance between convective and diffusive transport

In a steady state, the net diffusive and convective transport of enthalpy and solute through any horizontal cross-section in the cavity balance each other out exactly, this is expressed by:

$$\int_{r_i}^{r_o} W\theta r \, dr = \alpha' \int_{r_i}^{r_o} r \, dr = 2\alpha'(1+1/\gamma) \tag{28}$$

$$\int_{r_i}^{r_o} W\phi r \, dr = 2\frac{\beta'}{Le}(1+1/\gamma). \tag{29}$$

Noting that the left-hand-side of equations (28) and (29) are constants, the right hand must also be; we then have $\alpha = az$ and $\beta = b\,Le\,z$, a and b being two constants.

Finally, the linear system of second-order coupled differential equations:

$$W - Ra_T(\theta + N\phi) = k \tag{30}$$

$$aW = \Delta_r \theta \tag{31}$$

$$b\,Le\,W = \frac{1}{Le}\Delta_r \phi \tag{32}$$

coupled to boundary conditions (24) and the integral conditions coming from (25)–(29):

$$\int_{r_i}^{r_o} W(r) r \, dr = 0, \quad \int_{r_i}^{r_o} \theta(r) r \, dr = 0, \quad \int_{r_i}^{r_o} \phi(r) r \, dr = 0 \tag{33}$$

$$\int_{r_i}^{r_o} W\theta r \, dr = 2a\left(1+\frac{1}{\gamma}\right) \quad \text{and} \quad \int_{r_i}^{r_o} W\phi r \, dr = 2b\left(1+\frac{1}{\gamma}\right) \tag{34}$$

define a simple, well-posed mathematical problem that can be solved rather easily.

4.3. Resolution

First of all, the value of constant k can be readily determined by integrating expression (30) through a horizontal cross-section, which, in view of the integral conditions (33), gives $k = 0$. Equation (30), therefore, reduces to:

$$W - Ra_T(\theta + N\phi) = 0. \tag{35}$$

4.3.1. Determination of the velocity

Substitution of (31) and (32) into the derivative of equation (30) gives the equation for velocity:

$$\Delta_r W - \omega^2 W = 0 \quad \text{with } \omega^2 = Ra_T(a + Nb\,Le^2). \tag{36}$$

This represents a Bessel equation. Its solution, assuming that ω is positive, is:

$$W(r) = C_1 I_o(\omega r) + C_2 K_o(\omega r) \tag{37}$$

where I_n and K_n are the modified Bessel functions of nth order [29].

(The case of a negative ω value brings no solution for the problem under consideration.) In terms of the yet unknown constant ω, C_1 and C_2 can readily be determined by deriving the velocity expression (37) and introducing the boundary conditions (24).

Hence the expressions for the constants are:

$$C_1 = \frac{Ra_T(1+N)}{\omega\Gamma}\left(K_1(\omega r_o) - \frac{1}{2\gamma+1}K_1(\omega r_i)\right)$$

$$C_2 = \frac{Ra_T(1+N)}{\omega\Gamma}\left(I_1(\omega r_o) - \frac{1}{2\gamma+1}I_1(\omega r_i)\right)$$

where $\Gamma = I_1(\omega r_i)K_1(\omega r_o) - I_1(\omega r_o)K_1(\omega r_i)$.

Note that these values of C_1 and C_2 also implicitly satisfy conservation of mass, i.e.

$\hat{W}(r_o) = \hat{W}(r_i)$ with the notation $\hat{W}(r) = \int W(r) r \, dr$.

4.3.2. Determination of temperature and concentration

Eliminating velocity from equations (31) and (32) gives a relation between θ and ϕ which gives, after two successive integrations,

$$a\phi - b\,Le^2\theta = D_1 \ln r + D_2. \tag{38}$$

The two constants D_1 and D_2 are obtained implying the use of boundary conditions (24) and integral conditions (33), respectively, in the resolution.

$$D_1 = \frac{a - b\,Le^2}{\gamma} \quad D_2 = \frac{-D_1}{4}\left(\frac{r_o^2 \ln r_o - r_i^2 \ln r_i}{1+1/\gamma} - 2\right).$$

Finally, the use of the first relation between θ and ϕ coming from Darcy's equation (36) implies:

$$\theta(r) = \frac{1}{\omega^2}(aW(r) - N\,Ra_T(D_1 \ln r + D_2)) \tag{39}$$

and

$$\phi(r) = \frac{1}{\omega^2}(b\,Le^2\,W(r) + Ra_T(D_1 \ln r + D_2)). \tag{40}$$

4.3.3. Completion of the solution

The last task is to determine the values of constants a and b, using the additional transport conditions. Introducing the last results concerning θ and ϕ into equations (34) and taking into account relations (35) and (38) the system reduces to:

$$\int_{r_i}^{r_o} W^2(r) r\,dr = 2Ra\left(1+\frac{1}{\gamma}\right)(a+Nb)$$

$$\text{and} \quad D_1 \int_{r_i}^{r_o} W(r) r \ln r\,dr = 2ab\left(1+\frac{1}{\gamma}\right)(1-Le^2). \tag{41}$$

Using the integral properties of Bessel's functions [29], that lead to the non-linear and coupled system of algebraic equations, we obtain:

$$\frac{r_o^2}{2}W^2(r_o) - \frac{r_i^2}{2}W^2(r_i) = 2Ra_T\left(1+\frac{1}{\gamma}\right)(a+Nb) \tag{42}$$

$$\frac{D_1}{\omega^2}\left(Ra_T(1+N)\frac{\ln(2\gamma+1)}{\gamma} - W(r_o) + W(r_i)\right) = 2ab\left(1+\frac{1}{\gamma}\right)(1-Le^2). \tag{43}$$

This system can readily be solved to obtain a and b as functions of (γ, Ra_T, Le, N).

Obviously, for the general case, the equation system defined by (42) and (43) has to be solved by numerical methods, e.g. by Newton–Raphson's method. Moreover, this is by far a much easier and faster task than numerically solving the full set of non-linear and coupled partial differential equations (10)–(13).

In this way, equations (37), (39) and (40) then give the velocity, temperature and concentration profiles.

Once the solution has been fully determined, it is possible to compute the average Nusselt and Sherwood numbers on the inner wall, which are usually of interest in engineering applications, as mentioned in Section 3:

$$Nu_i = \frac{\ln(2\gamma+1)}{\gamma}(\theta(r_o) - \theta(r_i))^{-1}$$

$$Sh_i = \frac{\ln(2\gamma+1)}{\gamma}(\phi(r_o) - \phi(r_i))^{-1}. \tag{44}$$

Note that because the wall-to-wall concentration and temperature differences at any arbitrary horizontal cross-section are independent of the vertical position of the cross-section, in the domain of validity of the analytical solution, the analytical expressions for *Sh* and *Nu* do not depend on the height of the enclosure, but still depend entirely on the curvature of the cylinders.

4.3.4. Limit cases

When ω becomes high, an asymptotic analysis of the modified Bessel functions [29] enables the reduction of the analytical solution presented in the foregoing section to:

$$W(r) \approx \frac{Ra_T(1+N)}{\omega\gamma\sqrt{r}}\left(\frac{e^{\omega(r-r_o)}}{\sqrt{r_o}} - \frac{e^{\omega(r_i-r)}}{\sqrt{r_i}}\right).$$

In this case, the velocities at the inner and outer cylinders and the side-to-side temperature and concentration differences are expressed by very simple expressions depending on ω and D_1 which are the solutions of a polynomial system coming from equations (41), much easier to solve than the previous one.

We can then readily deduce the Nusselt and Sherwood numbers, which are based on the temperature and concentration differences between the vertical boundaries described in (44).

Moreover, it is possible to simplify the analytical solution further by additional assumptions about input parameters (γ, Ra_T, Le, N). Consider, for example, the case of a heat-driven boundary layer. It is then assumed that fluid flow is mainly due to the gradients of temperature, i.e. $|N| \ll 1$. Under these circumstances, the approximate solution to equations (42) and (43) becomes $\omega = Ra_T^{2/5}\,2^{-1/5}(2\gamma+1)^{-1/5}$, yielding the following approximate values for the Nusselt number:

$$Nu_i = \ln(2\gamma+1)\,Ra_T^{2/5}(2\gamma+1)^{4/5}2^{-6/5}\gamma^{-1}(\gamma+1)^{-1}.$$

The thickness of the hydrodynamic, concentration and temperature boundary layers along the inner and outer cylinders can then be estimated by: $(\delta r)_i = (\delta r)_o/(2\gamma+1) \approx 1/\omega$.

It should be noted that this behaviour is exactly what was predicted by some other studies in natural convection with this geometry [23].

5. Results and discussion

5.1. Numerical results

A large number of numerical computations of the full mathematical problem have been carried out with the

main objective of investigating the steady-state behaviour of the problem considered here. The best way to estimate the heat and mass transfer engineering contribution is to evaluate the expressions for overall Nusselt and Sherwood numbers. That is why we systematically investigated the effect of each dimensionless parameter on these numbers, for different values of the curvature.

5.1.1. Influence of the aspect ratio

The first step consists of bringing out the influence of the aspect ratio on the mixture behaviour.

It is already known that when the cavity is tall enough, provided that the end effects are confined to small regions adjacent to the top and bottom of the cell, the flow presents a parallel boundary-layer structure.

In order to show this trend more precisely, the influence of the aspect ratio on the average Nusselt and Sherwood numbers at the inner wall is illustrated in Figs 3(a) and (b). Therefore, these figures represent Nu_i(a) and Sh_i(b) defined in formulae (19) and (20) for A varying from 1–10 and for different values of γ, the other parameters being fixed at $Ra_T = 100$, $Le = 10$ and $N = 1$.

They clearly exhibit that the Nusselt and Sherwood numbers lead asymptotically to a constant value, whatever the curvature. These constant values, plotted in grey in the figures, come from the analytical study developed in Section 4 and will be discussed later, in Section 5.2.

These figures also represent the temperature (a) and concentration (b) fields for limiting cases ($A = 1$, 10 and $\gamma = 0$, 10). They illustrate the stratification of the flow as A increases. We can observe that unlike in the Cartesian case ($\gamma = 0$), the cylindrical case does not present a centro-symmetrical distribution of the fields. This is due to the non-symmetrical form of the equations in the radial direction, as well as the boundary conditions.

In order to present a large amount of data within reasonable space and at the same time satisfy the preoccupations of engineering applications, in the following parts we focus on the study of the influence of the physical–chemical input parameters (Ra_T, Le, N) on the overall Nusselt and Sherwood numbers.

5.1.2. Influence of the Rayleigh number

While it is well known that the Rayleigh number characterizes the influence of the external forces on the convective motion, it can be seen in Fig. 4 that the Nu_i (a) and Sh_i (b) numbers, i.e. heat and solute transfer rate on the vertical inner wall, increase with the Rayleigh number. Thus, the mixture is carried by the general convective movement whose strength increases with the Rayleigh number, velocity being more important near the inner cylinder than the outer cylinder. On the other hand, when the Rayleigh number is equal to zero, there is no convection and the mixture is submitted to the so-called pure diffusive regime. Here, there is an exact solution of the system (10)–(15) for the temperature and the concentration which is linear for the rectangular case, and logarithmic for the cylindrical case, as can be seen in the fields plotted in Figs 4(a) and (b).

5.1.3. Influence of the Lewis number

The influence of the Lewis number on Nu_i and Sh_i numbers is represented in Fig. 5(a) and (b). The Lewis number is the ratio of thermal to solutal diffusivities,

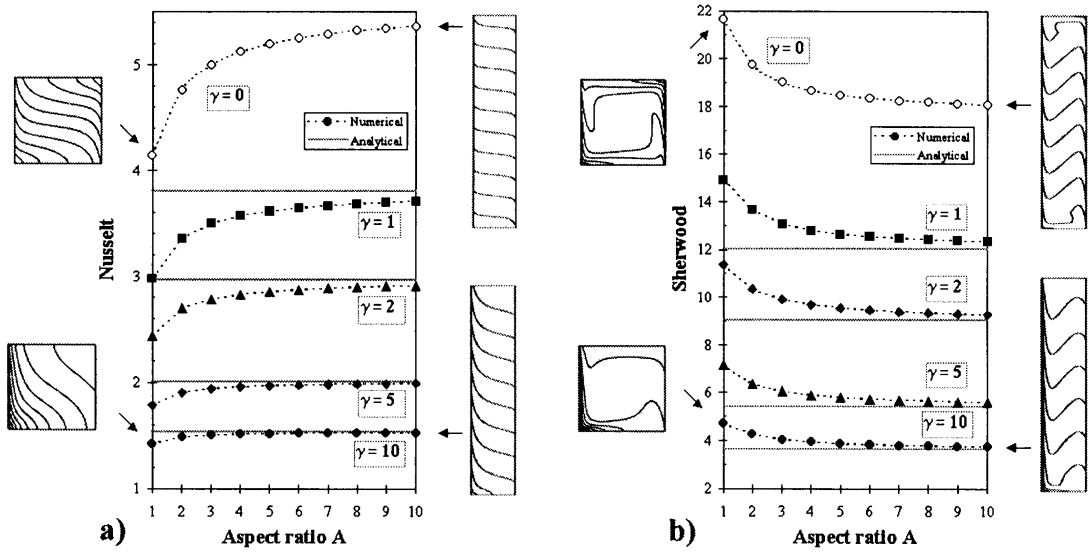

Fig. 3. Influence of the aspect ratio A on the Nu_i (a) and Sh_i (b) for different values of γ. Isotherms (a) and isohalines (b) at steady-state for $Ra_T = 100$, $Le = 10$, $N = 1$, $A = 1$ and 10, $\gamma = 0$ and 10.

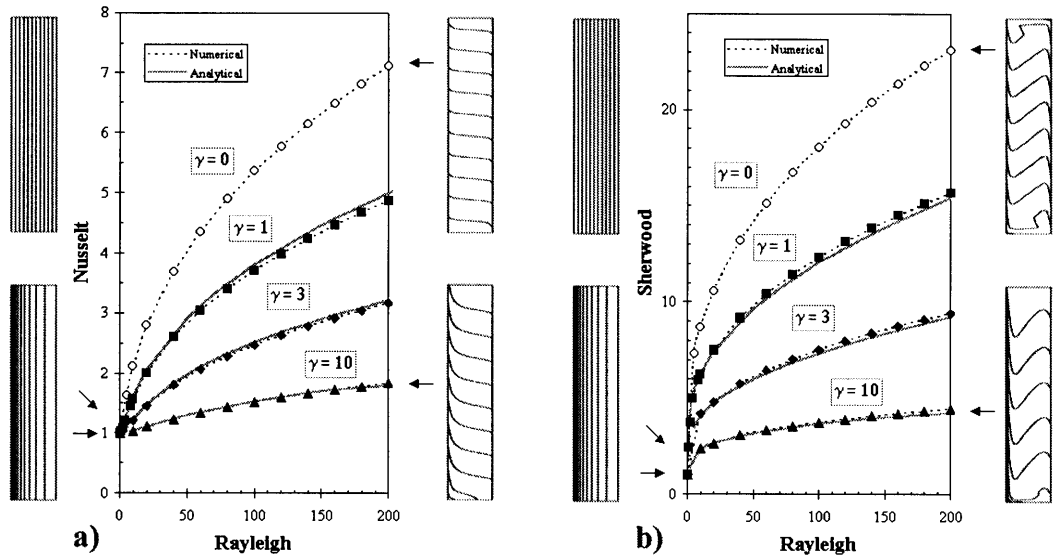

Fig. 4. Influence of the Rayleigh number Ra_T on the Nu_i (a) and Sh_i (b) for different values of γ. Isotherms (a) and isohalines (b) at steady-state for $A = 10$, $Le = 10$, $N = 1$, $Ra_T = 0$ and 200, $\gamma = 0$ and 10.

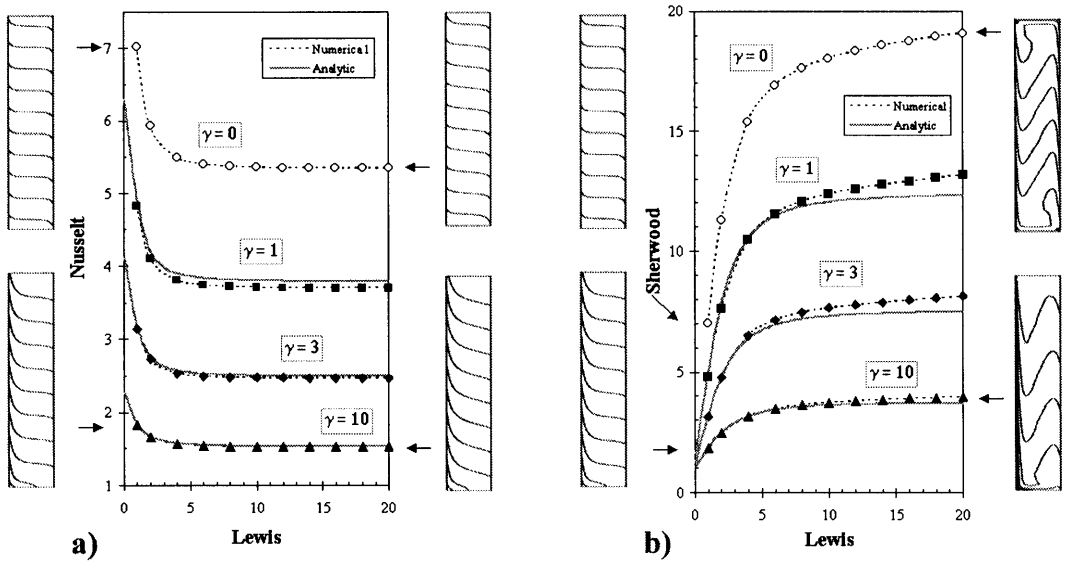

Fig. 5. Influence of the Lewis number Le on the Nu_i (a) and Sh_i (b) for different values of γ. Isotherms (a) and isohalines (b) at steady-state for $A = 10$, $Ra_T = 100$, $N = 1$, $Le = 1$ and 20, $\gamma = 0$ and 10.

so it characterizes solute transport relative to thermal diffusion. When the Lewis number is equal to unity, solute and heat diffuse in equal proportions, leading to exactly identical temperature and concentration fields in the steady state, as plotted in Fig. 5. Note that in this case, which generally concerns gases, the duration of the transient state is shorter for the concentrations than for the temperature, due to normalized porosity $\varepsilon^* < 1$.

Regarding liquids, heat diffusion is always much stronger than mass diffusion, leading to Lewis numbers much greater than 1. It can be seen in Fig. 5 that when the Lewis number increases, Nu_i becomes constant and

Sh_i increases. For $Ra_T = 100$ and $Le = 20$, as in the limit case plotted in Fig. 5, the temperature distribution is fully stratified, while concentration distribution is hardly stratified at all. For higher Lewis numbers, the core of concentration field is in a state of almost uniform concentration.

5.1.4. Influence of the buoyancy ratio

The non-dimensional parameter N characterizes the ratio between solutal and thermal buoyancy forces. Its influence on the Nu_i and Sh_i numbers is represented in Figs 6(a) and (b) respectively, for $A = 10$, $Ra_T = 100$ and $Le = 10$.

It shows that beneath unity, the Nusselt and Sherwood numbers are almost constant, independently of the curvature. This means that for these values, the solutal contribution is less than the thermal one, and becomes negligible as N becomes smaller, leading to a heat-driven regime. Similarly, as N increases, the solutal contribution is no longer negligible, and co-operates with the thermal contribution to increase the convective amplitude and converge to a steady-state different from the previous one, as shown in the fields plotted in Figs 6(a) and (b). This could lead, as N becomes high, to a situation where the solutal force prevails: the regime becomes solute-driven.

N can also be negative, depending on the value of the concentration expansion coefficient β_c. In this case of opposing buoyancy forces, oscillating regimes may appear. This behaviour has been investigated by Alavyoon et al. [10] for rectangular cavities. This also holds in cylindrical configurations. These regimes, being unsteady, prevent the formation of parallel structure.

5.1.5. Influence of the curvature

The present results, obtained for a wide range of Ra_T, Le, N and γ, also show the effect of curvature on convective heat and mass transfer. It should be noticed that the results concerning the case of $\gamma = 0$ came from the numerical resolution for the problem in a rectangular cavity and are in good agreement with the limiting case of the annular problem. Flow pattern, temperature and concentration fields for some typical values ($Ra_T = 100$, $Le = 10$, $N = 1$ and $\gamma = 0, 10$) are reported in Fig. 7 in order to emphasize the influence of the curvature illustrated in the previous figures. It stresses that as γ increases, isotherms and isohalines shift towards the inner wall, resulting in asymmetry of the temperature and concentration fields in the annulus. Furthermore, the temperature and concentration gradients near the inner wall increase rapidly as the influence of the curvature increases and the behaviour is just the reverse of that near the outer wall.

This influence of curvature is therefore felt by the Nusselt and Sherwood numbers and is also summed up in Fig. 7. So, the presence of a cylindrical geometry implies a decrease of the average Nusselt and Sherwood numbers at the inner cylinder and their increase at the outer cylinder. It should be noticed that because of the definition of the Nusselt and Sherwood numbers [(19) and (20)], their expression also depends on the curvature being weighted

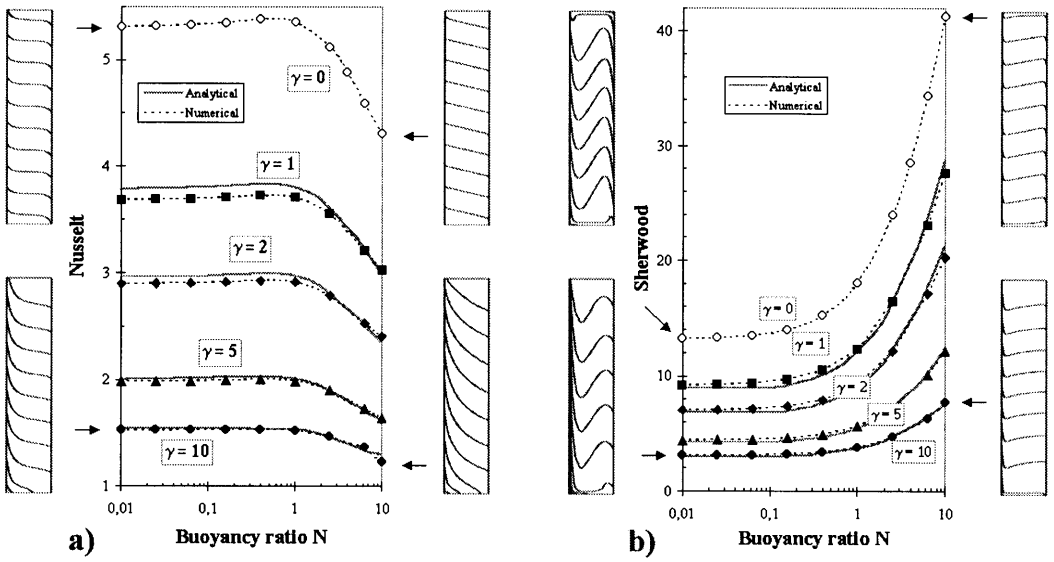

Fig. 6. Influence of the buoyancy ratio N on the Nu_i (a) and Sh_i (b) for different values of γ. Isotherms (a) and isohalines (b) at steady-state for $A = 10$, $Ra_T = 100$, $Le = 10$, $N = 0.01$ and 10, $\gamma = 0$ and 10.

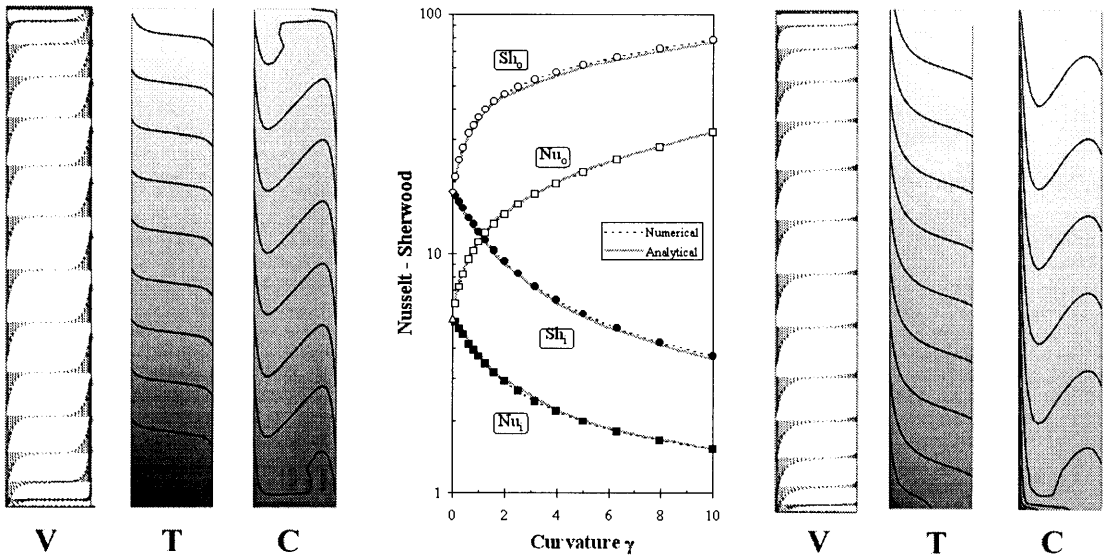

Fig. 7. Influence of the curvature parameter γ on the average Nusselt and Sherwood numbers on the inner and outer cylinders. Pattern of velocity vectors, isotherms and isohalines at steady-state for $A = 10$, $Ra_T = 100$, $Le = 10$, $N = 1$, $\gamma = 0$ and 10.

by $\ln(2\gamma+1)/\gamma$ for the inner values and by $(2\gamma+1)\ln(2\gamma+1)/\gamma$ for the outer value.

5.2. Analytical results

With a view to illustrate the crucial features and the domain of the validity of the steady-state analytical solution, as well as the curvature effects on the mixture's flow, analytical results were also represented by a grey line on the numerical results (Figs 4–7), for they cover a wide range of parameters.

The assumption used in the implementation of the analytical solution is that the flow presents a parallel boundary-layer structure. The validity of this assumption improves steadily as the cavity becomes taller, provided that the end effects are confined to small regions adjacent to the top and bottom of the cell. For a given set of (γ, Ra_T, Le, N) the analytical Nusselt and Sherwood numbers have a constant value, independently of the aspect ratio A. The parallel-flow model will then be valid as soon as the analytical solution is close enough to the numerical one.

Thus, as in Fig. 3, when $A \geqslant 5$, the flow can be considered as parallel, and the analytical solution satisfactorily agrees with the numerical results.

The numerical study of the influence of the physical–chemical properties, controlled by the non-dimensional parameters (Ra_T, Le, N), and the curvature, controlled by γ, presented in Figs 4–7, was carried out for an aspect ratio of 10. In the domain covered by these results, i.e. $1 \leqslant Ra_T \leqslant 200$, $1 \leqslant Le \leqslant 20$, $0.01 \leqslant N < 10$ and $0 \leqslant \gamma \leqslant 10$, the results obtained by numerical and analytical resolution are very close. This shows that the analytical solution is quite efficient to describe the behaviour of the mixture in a cylinder submitted to heat and mass fluxes for aspect ratios greater than 5. For higher Rayleigh or Lewis numbers, convection becomes so strong and mass diffusion so weak that the stratification assumption is no longer valid for the temperature and concentration distributions.

Finally, Fig. 8 represents numerical (dotted line) and analytical profiles (grey line) of velocity, temperature and concentration at mid-height ($z = 0$) for $A = 10$, $Ra_T = 100$, $Le = 10$ and $N = 1$. It allows a more accurate comparison between numerical and analytical solutions in the steady state. The agreement between the two is also shown to be good too. It should be noted that, as already observed with the numerical simulation, an increase in the curvature parameter γ introduces a decrease in temperature and concentration which is much faster near the outer wall and much slower near the inner wall.

6. Conclusion

In this paper the phenomenon of natural double-diffusive convection was studied through a vertical saturated porous annulus subjected to uniform fluxes of heat and mass. The formulation of the problem was developed on the basis of a two-dimensional mathematical model associated to Darcy's law with Boussinesq approximation.

In order to obtain detailed results for temperature and

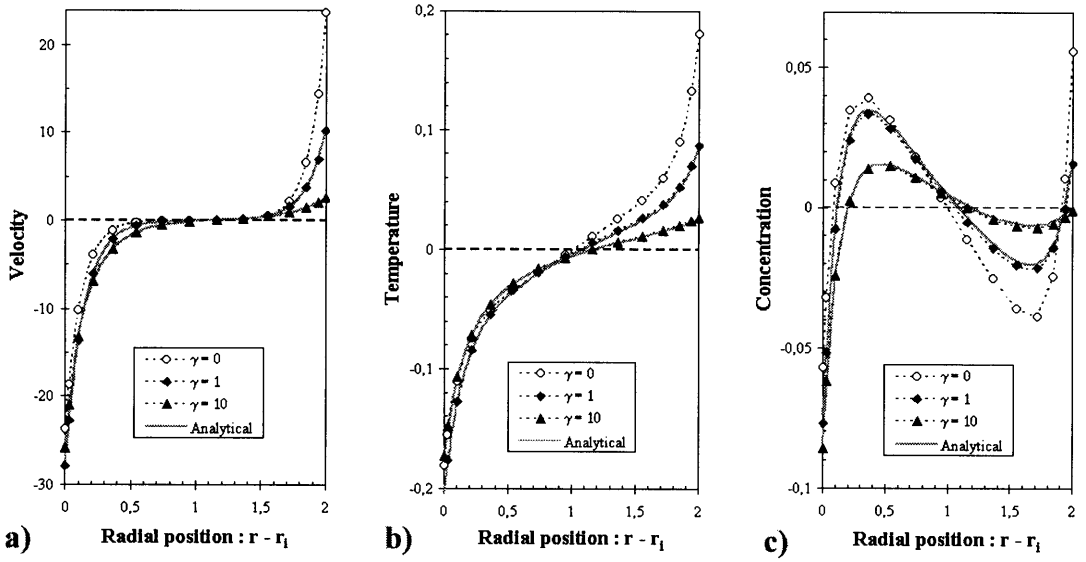

Fig. 8. Comparison between fully numerical (dotted lines) and analytical (grey lines) solutions at steady-state for $A = 10$, $Ra_T = 100$, $Le = 10$ and $N = 1$ for different values of γ. Velocity (a), temperature (b) and concentration (c) profiles at mid-height ($z = 0$).

solute distributions for the convective flow, a numerical solution was developed, and an extensive set of numerical simulations carried out to cover the parametric domain in which double-diffusive convection can exist. The effects of the major system parameters on the double-diffusion were investigated. The brief summary of the results is:

—Curvature effects on temperature, concentration and velocity fields are significant and strongly disturb the centro-symmetrical nature of the flow obtained in a rectangular cavity.

—The numerical integration of the full problem reveals that for sufficiently large aspect ratios, the flow is almost parallel except in regions close to the horizontal boundaries, and the concentration and temperature fields in the core region are rather linearly stratified.

—The assumption of parallel flow allows analytical resolution of the steady-state problem and leads to relatively simple solutions, less time-consuming than the numerical ones. These solutions can be even simpler for limit cases like $Ra_T \gg 1$ and solute-driven or heat-driven boundary layer approximations.

—A good agreement is found between analytical and numerical results for $A = 10$, $1 \leqslant Ra_T \leqslant 200$, $1 \leqslant Le \leqslant 20$, $0.01 \leqslant N \leqslant 10$ and $0 \leqslant \gamma \leqslant 10$.

Finally, it should be noted that the analytical solution developed in this study is quite accurate in predicting the flow structure and heat and mass transfer for a wide range of parameters and for sufficiently high aspect ratios. It is therefore a powerful tool of analysis.

Acknowledgement

Most of the computational work was carried out on the SP2 Cluster of the National Computational Centre of Montpellier (C.N.U.S.C.).

References

[1] M.A. Combarnous, S.A. Bories, Hydrothermal convection in saturated porous media, Adv. Hydrosci, vol. 10, Academic Press, 1975, pp. 231–307.

[2] D.A. Nield, A. Bejan, Convection in Porous Media, Springer Verlag, New York, 1992.

[3] O.V. Trevisan, A. Bejan, Combined heat and mass transfer by natural convection in porous medium, Adv. Heat Transfer 20 (1990) 315–352.

[4] G.Z. Gershuni, E.M. Zhukhovitskii, D.V. Lyubimov, Stability of stationary convective flow of a mixture in a vertical porous layer, Fluid Dyn. 15 (1980) 122–127.

[5] A.A. Khan, A. Zebib, Double-diffusive instability in a vertical layer of porous medium, J. Heat Transfer 103 (1981) 179–181.

[6] A. Bejan, K.R. Khair, Heat and mass transfer by natural convection in a porous medium, Int. J. Heat Mass Transfer 28 (1985) 909–918.

[7] O.V. Trevisan, A. Bejan, Mass and heat transfer by natural convection in a vertical slot filled with porous medium, Int. J. Heat Mass Transfer 29 (1986) 404–415.

[8] Z. Zhang, A. Bejan, The horizontal spreading of thermal

and chemical deposits in a porous medium, Int. J. Heat Mass Transfer 30 (1987) 2289–2303.
[9] F. Alavyoon, On natural convection in vertical porous enclosures due to prescribed fluxes of heat and mass at the vertical boundaries, Int. J. Heat Mass Transfer 36 (1993) 2479–2498.
[10] F. Alavyoon, Y. Masuda, S. Kimura, On natural convection in vertical porous enclosures due to opposing fluxes of heat and mass prescribed at the vertical walls, Int. J. Heat Mass Transfer 37 (1994) 195–206.
[11] K.W. Lin, Unsteady natural convection heat and mass transfer in a saturated porous enclosure, Wärme- und Stoffübertragung 28 (1993) 49–56.
[12] M. Mamou, P. Vasseur, E. Bilgen, D. Gobin, Double-diffusive convection in an inclined slot filled with porous medium, European J. Mech. 14 (1995) 629–652.
[13] M. Mamou, M. Vasseur, E. Bilgen, Multiple solutions for double-diffusive convection in a vertical porous enclosure, Int. J. Heat Mass Transfer 38 (1995) 1787–1798.
[14] M. Mamou, M. Vasseur, E. Bilgen, Thermosolutal convection instability in a vertical porous layer, Second Int. Thermal Energy Congress, Agadir, 1995, pp. 463–467.
[15] M. Marcoux, M. Karimi-Fard, M. C. Charrier-Mojtabi, Naissance des régimes de double-diffusion convectifs dans une cellule rectangulaire poreuse soumise à des flux de chaleur et de masse, 8èmes Journées Internationales de Thermique, Marseille, 1997.
[16] M.A. Havstad, P.J. Burns, Convective heat transfer in a vertical cylindrical annuli filled with a porous medium, Int. J. Heat Mass Transfer 25 (1982) 1755–1766.
[17] C.E. Hickox, D.K. Gartling, A numerical study of natural convection in a vertical annular porous layer, ASME Paper No. 82-HT-68, 1984.
[18] D.C. Reda, Natural convection experiments in a liquid saturated porous medium bounded by vertical coaxial cylinders, J. Heat Transfer 105 (1983) 795–802.
[19] V. Prasad, F.A. Kulacki, Natural convection in a vertical porous annulus, Int. J. Heat Mass Transfer 27 (1984) 207–219.
[20] V. Prasad, F.A. Kulacki, Natural convection in a porous media bounded by short concentric vertical cylinders, J. Heat Transfer 107 (1985) 147–154.
[21] V. Prasad, F.A. Kulacki, M. Keyhani, Natural convection in porous media, J. Fluid Mech. 150 (1985) 89–119.
[22] V. Prasad, F.A. Kulacki, A.V. Kulkarni, Free convection in a vertical, porous annulus with constant heat flux on the inner wall—experimental results, Int. J. Heat Mass Transfer 29 (1986) 713–723.
[23] T.H. Nguyen, D.L. Nguyen, S. Lavoie, Convection naturelle dans un espace annulaire poreux soumis à un flux de chaleur constant, Ecole Polytechnique de Montréal, Rapport technique EP 86-1, 1986.
[24] M. Marcoux, J.K. Platten, G. Chavepeyer, M.C. Charrier-Mojtabi, Diffusion thermogravitationnelle entre deux cylindres coaxiaux: effet de la courbure, 2èmes Rencontres Int. de Thermodiffusion, Entropie 198/199 (1996) 89–96.
[25] M. Azaiez, C. Bernardi, M. Grundman, Spectral methods applied to porous media, East–West Num. Math. 2 (1994) 91–105.
[26] C. Canuto, M.Y. Hussaini, A. Quarteroni, T. Zang, Spectral Methods in Fluid Dynamics, Springer Verlag, New York, 1988.
[27] K. Arrow, L. Hurwicz, H. Uzawa, Studies in linear and non-linear programming, Stanford University Press, Stanford, 1958.
[28] T.A. Zang, M.Y. Hussaini, Fourier–Legendre spectral methods for incompressible channel flows, Proc. 9th Conf. on Numer. Methods in Fluid Dynamics, Saclay, 1984.
[29] W.W. Bell, Fonctions Spéciales à L'usage des Ingénieurs, Dunod, 1971, pp. 92–154.